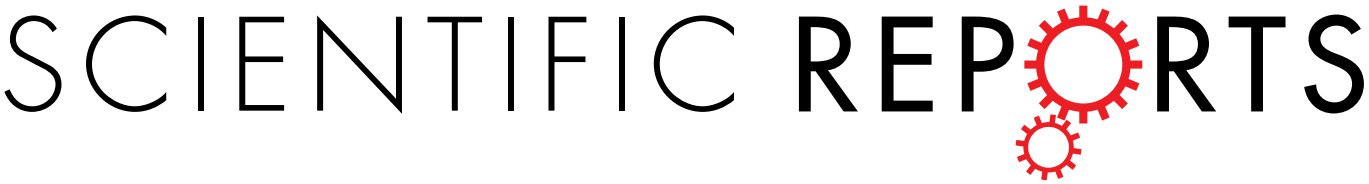

OPEN

Self-Assembled 3D Flower-Like Nickel Hydroxide Nanostructures and Their Supercapacitor Applications

Received: 29 March 2016
Accepted: 18 May 2016
Published: 02 June 2016

Nazish Parveen & Moo Hwan Cho

Three-dimensional (3D) nanostructures have attracted considerable attention because of their high surface areas and unique properties which gives outstanding performance in catalysis and energy storage applications. This paper proposes the growth mechanism of 3D flower-like β-$Ni(OH)_2$ constructed through a two dimensional sheet framework using a one-step oleylamine-assisted solvothermal approach, where oleylamine acts as the surfactant, co-solvent, stabilizer, and reducing agent. A detailed examination of the product morphology after various reaction times suggested that the self-assembly of flower occurs through a mechanism involving nucleation, Ostwald ripening, and recrystallization. The associated characterization revealed it to be pure β-$Ni(OH)_2$ without any sign of contamination. The effect of the morphology (sheet to 3D flower-like β-$Ni(OH)_2$) on the electrochemical supercapacitive behavior was assessed by cyclic voltammetry and galvanostatic charge-discharge tests. The results showed that 3D flower-like β-$Ni(OH)_2$ exhibited better specific capacitance of ~1567 F g^{-1} at a current density of 1 A g^{-1} and retained ~25% capacitance at a high current density of 10 A g^{-1} compared to the other reference materials. The superior electrochemical properties of the 3D flower-like β-$Ni(OH)_2$ originate from their large specific surface area and unique structure.

Supercapacitors or electrochemical capacitors have attracted considerable attention for novel energy storage devices because they can immediately provide a higher power density with simultaneously shorter charging times than batteries, and a higher energy density than conventional dielectric capacitors[1–4]. Therefore, supercapacitors are considered promising energy storage devices and power supplies for digital products, hybrid electric vehicles, and other portable electronic devices that require a high power density and long cycle life[1–3]. In general, supercapacitors can be divided into the following two types according to their energy storage mechanism: electrical double layer capacitors (EDLC) typically made from carbon or graphene based materials, which work on rapid ion adsorption/desorption; and pseudocapacitors originating from fast faradaic charge transfer reactions similar to the processes observed in batteries[2,3]. Pseudocapacitors using transition-metal oxides and electronically conducting polymers as active materials can be used to produce asymmetrical supercapacitors with both improved energy and power densities[5,6].

Earlier in supercapacitor applications, a range of metal oxides were used as electrode materials. Among them ruthenium oxide (RuO) is used widely as an electrode material because of its high theoretical capacitance (1500 Fg^{-1})[6]. On the other hand, the high cost and toxicity of RuO have limited its commercialization as a supercapacitive electrode material. Therefore, many studies have searched for alternative inexpensive electrode materials with good capacitive features, such as NiO, CoO_x, Mn_3O_4, MnO_2, CuO, $Co(OH)_2$, and $Ni(OH)_2$[7–9]. Among these metal oxides, $Ni(OH)_2$ has attracted more attention as an electrode material in energy and power storage devices, particularly for supercapacitors, because of its unique physical and chemical properties, such as natural abundance, high theoretical surface area, low cost, and well-defined electrochemical redox behavior[7,10,11]. On the other hand, most $Ni(OH)_2$-based electrodes have suffered from an inferior rate performance and poor cycle stability by possessing extremely attractive theoretical capacitance values. The utilization rate of the active materials and the electron and ion transmission rates determine the specific capacitance and rate performance of the supercapacitors, respectively. Therefore, the development and design of three dimensional structured materials have

School of Chemical Engineering, Yeungnam University, Gyeongsan, Gyeongbuk 712-749, South Korea. Correspondence and requests for materials should be addressed to M.H.C. (email: mhcho@ynu.ac.kr)

attracted considerable interest because they provide sufficient space and active sites for the interaction of electrolytes ions during the electrochemical process[12,13]. In addition, self-assembled micro/nano three-dimensional (3D) structures as electrode materials are some of the best systems in the area of supercapacitors[13,14]. These structures constructed with nanometer-scaled building blocks, including nanoparticles, nanorods, nanosheets etc., have the advantages of both the building blocks and assemblies. More importantly, the building blocks with a high specific surface area can guarantee more effective contact between the electrolyte and the active materials, hence increasing their utilization rate. The assembly, with its desirable and mechanical properties, guarantees good stability and practical fabrication[15–17]. Therefore, the development of a feasible and facile approach to manufacture morphology-controlled 3D flower-like β-$Ni(OH)_2$ structures consisting of a low-dimensional building block is desired. Over the past few years, a range of approaches have been developed to synthesize micro/nano-structures with complex morphologies. Of these, the hydrothermal or solvothermal method is considered to be efficient because the shape and size of materials is easy to control[18,19].

This paper reports a simple, cost effective, one-step oleylamine-assisted solvothermal approach for the synthesis of 3D flower-like β-$Ni(OH)_2$, where oleylamine acts as the surfactant, co-solvent, stabilizer, and reducing agent. The effects of the reaction time on the resulting morphology have been studied systematically to rationalize the structural configuration. The effects of morphology on the electrochemical performance were also examined. The results showed that the 3D flower-like β-$Ni(OH)_2$ electrode exhibited a high specific capacitance of 1567 F g^{-1} at a current density of 1 A g^{-1} and retained approximately 25% at a higher current density. The excellent capacitance of the 3D flower-like β-$Ni(OH)_2$ was attributed to a 3D flower-like structure, which provides a high surface area and shorter conduction length for electrolytic ions.

Results and Discussion

Morphological Analysis. Time-dependent experiments were conducted to understand the morphological changes and formation process of the 3D flower-like β-$Ni(OH)_2$. During the experiment the samples were collected at different time intervals and the morphological changes was carried out by scanning electron microscope (SEM) and transmission electron microscopy (TEM) analysis. The initial morphological investigation of the as-synthesized 3D flower-like β-$Ni(OH)_2$ for different reaction times was examined by SEM, which shows that the reaction time has a significant impact on the morphology of β-$Ni(OH)_2$. As shown in Figs 1a and S1a, at the early stage after 4 h, the sample showed a sheet like structure with the size of ~200 to ~600 nm with no indication of the formation of flower-like structures. As the reaction time was increased from 4 h to 8 h (Figs 1b,c and S1b), several sheets began to form a flower-like morphology and the sheets acted as petals sticking out from the central part of the flower, and fewer sheets or 'petals' engaged in the building of a flower. After a 12 h reaction (Figs 1d–f and S1c), the growth of the 3D structures appeared to be complete, and these were now filled with packed sheets or 'petals'. The colonial growth of these sheet or 'petals' produces flowers with compact constructions. These sheets or 'petals' are interconnected with each other and interlaced like petals on a flower. The surface of each petal is very smooth, probably due to Ostwald ripening. As described elsewhere, such nanosheet-based ordered 3D flowered structures allow high access of the electrolyte to the integrated nanosheets, which are essential for the decrease in interface contact resistance between the parallel directions of the electrodes and electrolyte[20]. An enlarged SEM image (Fig. 1f) of the $Ni(OH)_2$ synthesized for a reaction time of 12h clearly shows that the 3D flower-like morphology generates some porosity. This SEM image shows that structures are comprised favorably of densely packed and uniform sheets with a thickness of less than 100 nm. The entire evaluation processes illustrate the growth of $Ni(OH)_2$ to a 3D structure involving nucleation/growth[18,19], aggregation mechanisms[20,21], self-assembly, and Ostwald ripening[18,19,22].

Further TEM analysis was also performed to understand the construction of 3D flower-like β-$Ni(OH)_2$, texture, and crystalline behavior of β-$Ni(OH)_2$-4, β-$Ni(OH)_2$-8, and 3D flower-like β-$Ni(OH)_2$. Figure 2 shows TEM images of the β-$Ni(OH)_2$ after different solvothermal treatments, i.e., 4, 8, and 12 h. After 4 h (Figs 2a and S2a) sheet-like structures were observed with no indication of flower formation but after 8 h (Figs 2b and S2b–d), both 'petal' and sheet-like structures were observed, which indicates that the sheet began to convert to a petal-like structure. In addition, after 12 h (Figs 2c and S2e), the complete formation of 3D flower-like structure was observed and these arrangements were made up of distinguishable sheets or 'petals' with a width ranging from 5 to 30 nm. The sharp contrast among the dark edges of these petals and their faded area clearly confirm that the some porous structures are generated in the 3D flowers, which substantiates the compactness of the petals preferentially in the central region of the flower rather than in the exterior, indicating the density variations of the sheet inside the same porous structure. These features associated with the interweaving petal subunits showed good agreement with the SEM observations. Figure 2e presents a typical higher magnification TEM image of a piece of extended petals of the flower-like structures. An enlarged view in Fig. 2f clearly shows that the petals are thin. A close inspection of Fig. 2e revealed the lattice-resolved HRTEM images of the regional part surrounded by a red frame. The insets clearly show the atomic planes with a fringe spacing of ~0.27 nm. The corresponding SAED results (inset in Fig. 2f) present a ring like diffraction pattern of $Ni(OH)_2$ flowers, indicating the polycrystalline nature or structure. The chemical composition of these 3D flower-like β-$Ni(OH)_2$ was determined by elemental mapping and energy dispersive X-ray (EDX) analysis, as shown in Figs 2g–i and S3. Elemental mapping suggested the presence of Ni and O in the 3D flower-like β-$Ni(OH)_2$, and the EDX spectrum (Fig. S3) also showed only a Ni and O peak, which further confirmed that the 3D flower-like β-$Ni(OH)_2$ had been synthesized successfully using one-pot solvothermal method and would potentially exhibit superior performance in supercapacitor applications.

Growth mechanism for the formation of 3D flower-like β-$Ni(OH)_2$ structure. SEM and TEM indicated that the possible crystal formation and its growth of the β-$Ni(OH)_2$ as a 3D flower-like β-$Ni(OH)_2$ occurred in two stages. First, $Ni(OH)_2$ with a poor crystalline phase was developed via the initial reaction of all the precursor, i.e., $Ni(NO_3)_2.6H_2O$, ethanol, and oleylamine. Oleylamine acts as a surfactant, solvent, and reducing agent,

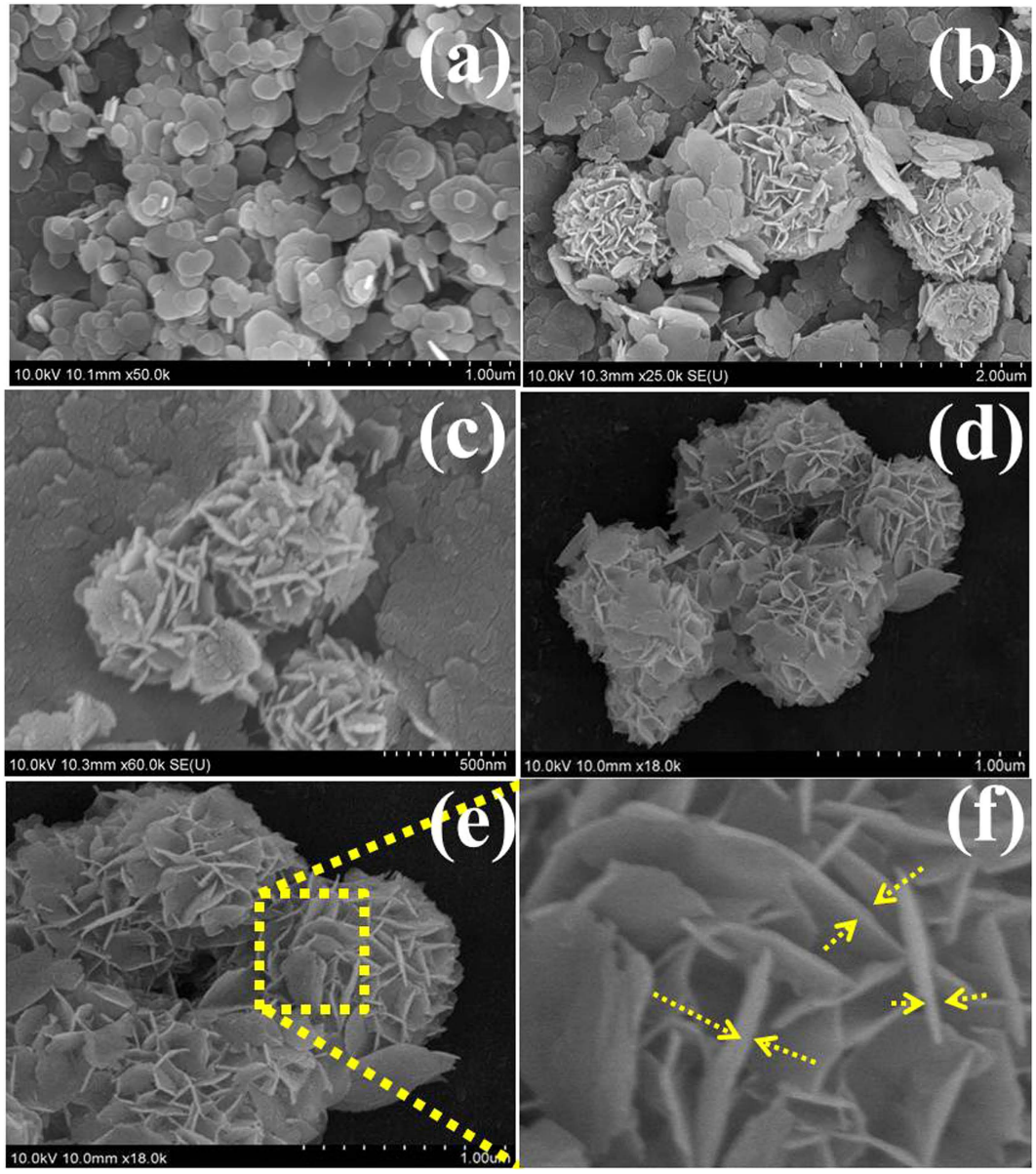

Figure 1. SEM images of the synthesized β-$Ni(OH)_2$ for different reaction times: after 4 h (**a**), 8 h (**b,c**) and (**d–f**) 12 h having fully grown flowers fabricated and packed nanopetals.

and forms complex compounds with the metal ions of the metal precursor, leading to metastable compounds that can act as secondary precursors.

The 3D flower-like morphology of the $Ni(OH)_2$ was attained simply by the changing the reaction duration i.e. from 4 h to 12 h. The $Ni(OH)_2$ obtained from the 4 h reaction time only showed a two-dimensional sheet-like morphology with a sheet size of 400 to 600 nm (Fig. 1a). When the reaction time was extended from 4 h to 8 h, several two-dimensional sheets began to convert to the flower morphology, as depicted in Fig. 1b. When the reaction time was increased to 12 h, the thickness of the interconnected was increased and the pore size of the surrounded petals decreased concomitantly, which led to the formation of compact three-dimensional flower structures (Fig. 1c). When the reaction time was prolonged, the size of the 3D structures increased and the morphology became a flower-like structure with a network of sheets on their surfaces, whereas after 12 h, the flower-like morphology gradually became more prominent[18]. These morphological changes from sheet to 3D flower-like structures indicate that the mechanism includes nucleation/growth[18,19], aggregation[20,21], self-assembly, and Ostwald ripening[18,19,22]. Among these, the Ostwald ripening and self-assembly played important roles to form the 3D flower-like structure of the $Ni(OH)_2$ from its initial crystal structure. In the Ostwald ripening process, flakes with larger size and small surface energy are thermodynamically favored and the dissolved tiny and unstable crystals provides the source material for the growth of flakes during the dissolution and recrystallization process. The dissolved nickel atoms may continuously attach and bond to the surface of larger flakes, and spread the (001) planes in order to achieve a minimum total free energy[23]. Overall, the larger flakes with low surface

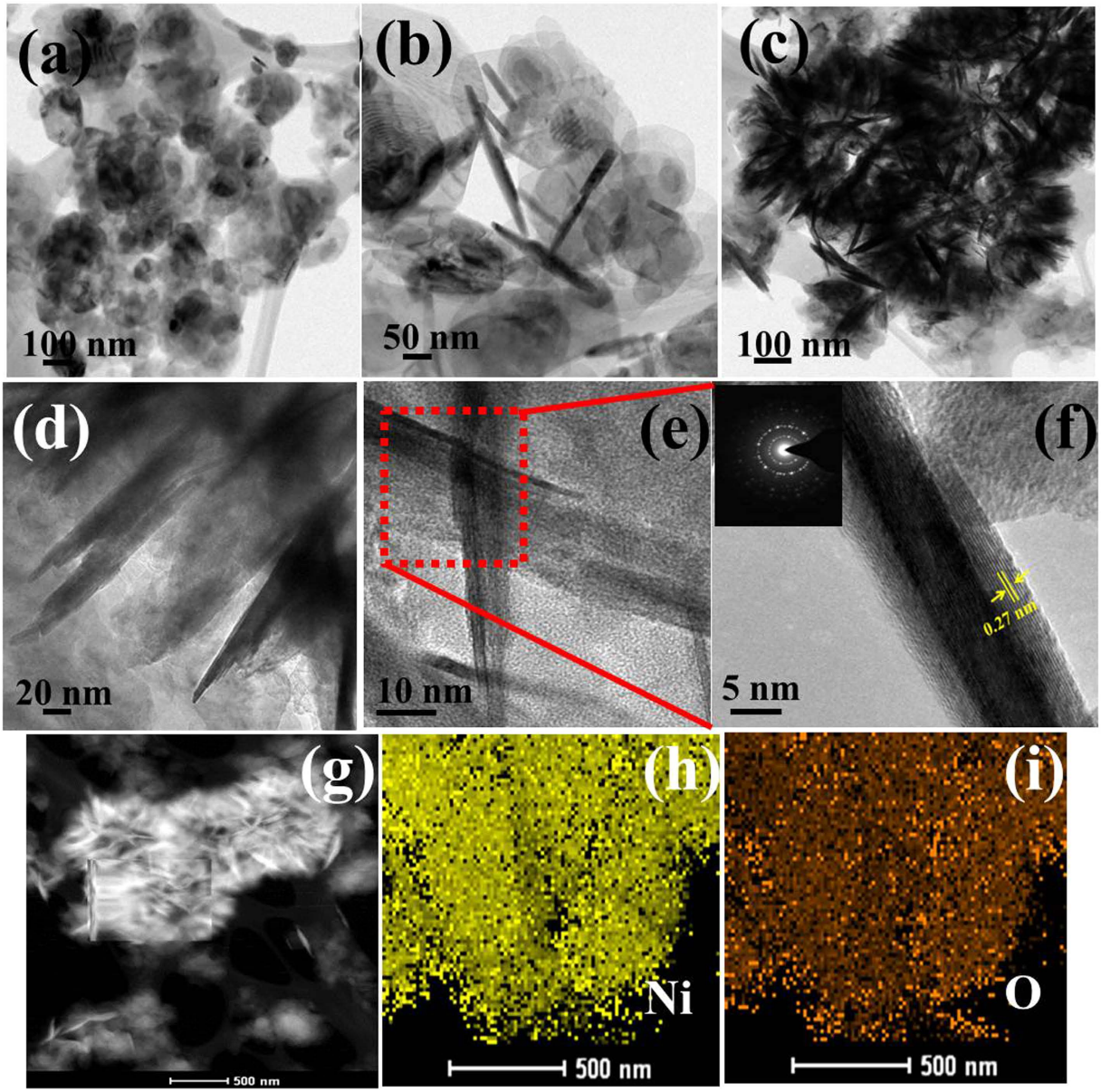

Figure 2. TEM images of the synthesized β-Ni(OH)$_2$ at different reaction times: after 4 h (**a**), 8 h (**b**), 12 h having grown flower-like structures fabricated with packed nanopetals (**c**), segment of a 3D flower (**d**), HRTEM image of intersecting nanopetals (**e**), enlarged view of the enclosed area (SAED pattern in inset) (**f**) and elemental mapping (**g–i**) of the 3D flowers after 12 h.

energy are thermodynamically favored and the unstable tiny crystals dissolved to provide the source material for the growth of flakes during the dissolution and recrystallization process. The dissolved nickel atoms may be able to attach continuously and bond to the surface of the larger flakes, and spread the (001) planes to reduce the total free energy[23]. A similar mechanism has also been reported for the synthesis of 3D structures that involve rapid nucleation followed by the slow aggregation and crystallization of the initial crystal structure[24]. Figure 3 presents the proposed growth mechanism of the 3D flower-like β-Ni(OH)$_2$.

Structural Analysis. Figure 4a presents the XRD patterns of the as-synthesized β-Ni(OH)$_2$ prepared by the solvothermal method for different reaction times (4, 8 & 12 h) at 180 °C. β-Ni(OH)$_2$-4, β-Ni(OH)$_2$-8, and 3D flower-like β-Ni(OH)$_2$ showed XRD peaks at ~19.15, 33.02, 38.49, 52.03, 58.94, 62.63, 69.27, 70.45, and 72.81° 2θ. The peak became more intense with increasing reaction time (4, 8 & 12 h). For 3D flower-like β-Ni(OH)$_2$, peaks at 19.15, 33.02, 38.49, 52.03, 58.94, 62.63, 69.27, 70.45, and 72.81° 2θ were assigned to the (001), (100), (101), (102), (110), (111), (200), (103) and (201) planes, respectively, which were in good agreement with the standard values (JCPDS file no. 14-0117). No obvious peak from other impurities, such as α-Ni(OH)$_2$, was observed, indicating the high purity of the synthesized product[25]. 3D flower-like β-Ni(OH)$_2$ could be indexed entirely to a C6-type structure with the crystal phase of β-Ni(OH)$_2$ having unit cell dimensions of $a_0 = 3.126$ Å and $c_0 = 4.605$ Å[24,26,27].

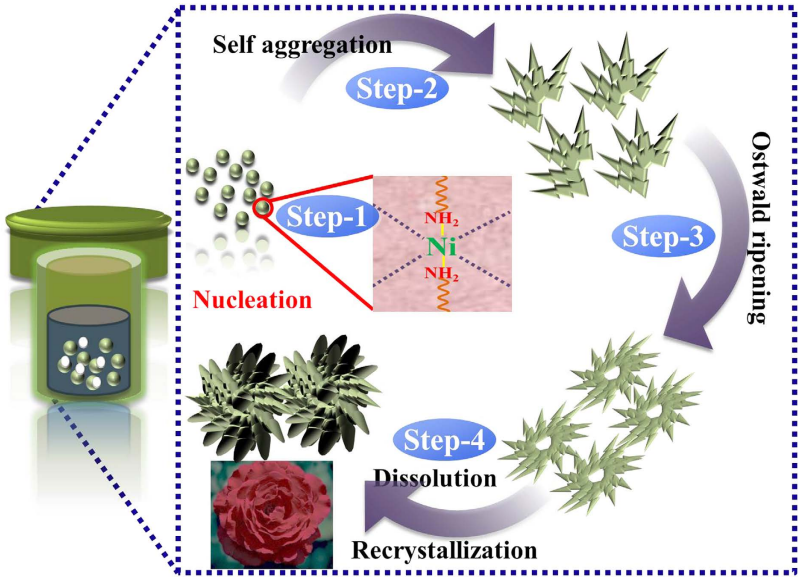

Figure 3. Schematic diagram of stepwise growth mechanism and morphological evolution of a 3D flower-like β-Ni(OH)$_2$ structure.

In addition, the (101) XRD peak for 3D flower-like β-Ni(OH)$_2$ was more intense compared to the (001) plane. This suggests that the sheets are grown preferentially along the (001) plane by Ostwald ripening. These XRD results are consistent with the previously reported articles[23].

FTIR spectroscopy was used to probe the major functional groups and the chemical interaction of the samples. Figure 4b shows the FTIR spectra of all the β-Ni(OH)$_2$ samples, in which the sharp band observed at ~3635 cm^{-1} was assigned to the stretching vibrational mode (ν-OH) of the non-hydrogen bonded hydroxyl groups, whereas the broad band at ~3495 cm^{-1} was attributed to the stretching mode of the hydrogen bonded hydroxyl groups in the Ni(OH)$_2$ structure. The peak at ~550 cm^{-1} was attributed to the in plane deformation vibrations of water (δ-OH). Weak bands were observed at ~2885 and ~2977 cm^{-1}, which were assigned to the symmetric and asymmetric stretching vibrations of the -CH$_2$- alkyl chain. The presence of these -CH$_2$- alkyl chain may be due to the use of oleylamine in the reaction as a surfactant and reducing agent[28].

Nitrogen adsorption-desorption isotherms were conducted to examine the structural characteristics and surface area of the β-Ni(OH)$_2$-4, β-Ni(OH)$_2$-8, and 3D flower-like β-Ni(OH)$_2$ in Figure S4. The BET surface area of the β-Ni(OH)$_2$-4, β-Ni(OH)$_2$-8, and 3D flower-like β-Ni(OH)$_2$ were ~38.9 m^2/g, ~40.8 m^2/g, and ~72.9 m^2/g, respectively. This confirms that the 3D flower-like β-Ni(OH)$_2$ possess a relative large specific surface area due to the well-defined interior spaces caused by the unique 3D flower-like ordered configuration, which is beneficial to the electrochemical property. Furthermore, the BET analysis clearly shows that the 3D flower β-Ni(OH)$_2$ has a two-fold higher surface area than β-Ni(OH)$_2$-4. Overall, the special 3D flower-like structure will provide sufficient space and network-like petals for the interaction and intercalation of the electrolytic ions during the electrochemical performance, which would be advantageous for enhancing the supercapacitive performance.

XPS was performed to determine the surface characteristics, chemical composition, i.e., types of carbon, oxygen and nickel bonds, as well as the percentage of oxygen and nickel present in the synthesized Ni(OH)$_2$-4, β-Ni(OH)$_2$-8, and 3D flower-like β-Ni(OH)$_2$. The XPS survey scans (Fig. 4c) provide a complete view of the surface elemental composition of the β-Ni(OH)$_2$ samples (4 h, 8 h, and 12 h); no impurities were observed on the Ni(OH)$_2$ surface. As shown in Fig. 4c, the survey spectra of Ni(OH)$_2$-4, β-Ni(OH)$_2$-8, and 3D flower-like β-Ni(OH)$_2$ confirm the presence of only Ni and O, which is consistent with the EDX and elemental mapping results. The high-resolution O 1s (Fig. 4d) and Ni 2p (Fig. 4e) fitted core-level spectra of the 3D flower-like β-Ni(OH)$_2$, and characteristic peaks of Ni 2p and O 1s spectra were assigned to Ni^{2+} and hydroxyl ions[29,30].

Figure 4d presents the fitted O 1s core level spectra of the 3D flower-like β-Ni(OH)$_2$, which shows the three distinct peaks at a binding energy of 530.76, 531.88, and 533.01 eV. The binding energy observed at 530.76 eV was assigned to the metal-bond in 3D flower-like β-Ni(OH)$_2$, whereas the high intensity peak observed at a binding energy of 531.88 eV was assigned to the Ni-(OH) bond. Similarly, the peak at a binding energy of 533.01 eV was assigned to the multiplicity of the physisorbed and chemisorbed water at or near the surface of β-Ni(OH)$_2$[29–32]. These results show that many adsorbed hydroxyl group are present on the Ni surface, which may help enhance the electrochemical performance of the materials.

The high resolution Ni 2p core-level spectrum (Fig. 4e) was obtained to provide more details of the nature of the chemical bonding and the types of nickel present on the β-Ni(OH)$_2$. The core-level spectrum of the Ni 2p was split into two major peaks at ~872.7 and ~855.1 eV, which were assigned to Ni 2p$_{1/2}$ and Ni 2p$_{3/2}$, respectively, with a spin energy separation of 17.6 eV. Satellite peaks (Ni 2p$_{1/2}$, satellite: ~876.8 and ~879.7 eV; Ni 2p$_{3/2}$, satellite: ~859.8 and ~862.1 eV) were also observed, which are associated with the two types of nickel species and were assigned to Ni(II) and Ni(III) ions[32].

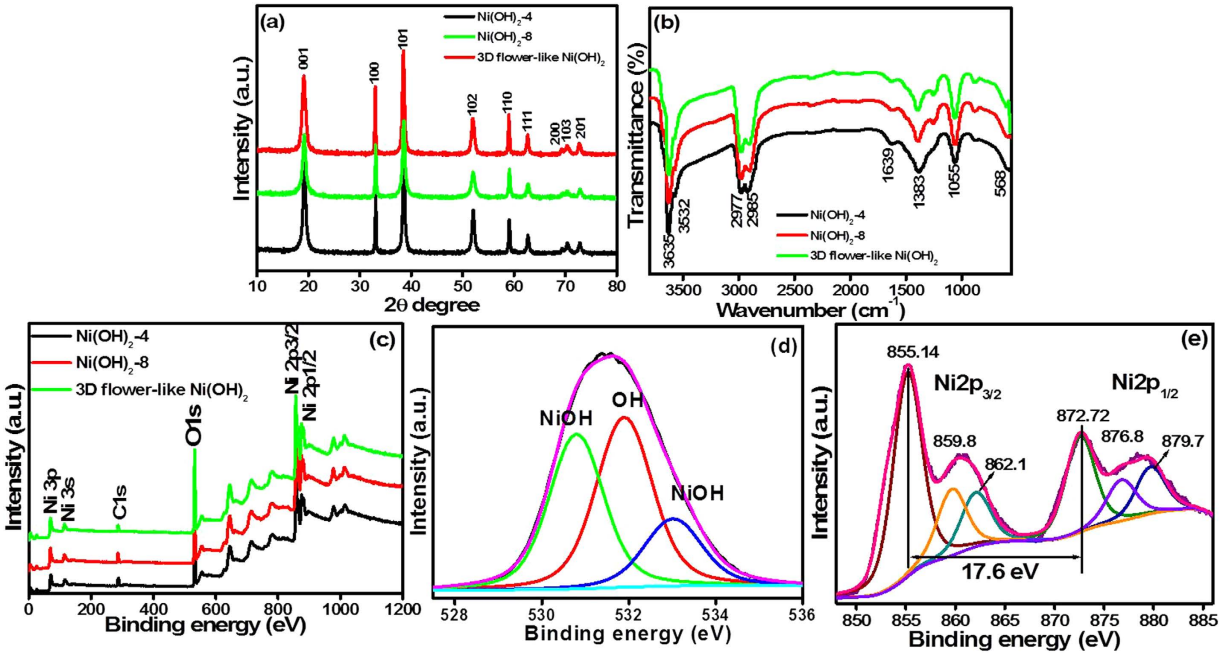

Figure 4. (**a**) XRD pattern, (**b**) FTIR analysis, (**c**) XPS survey spectra of the β-$Ni(OH)_2$-4, β-$Ni(OH)_2$-8 and 3D flower-like β-$Ni(OH)_2$, (**d**) O 1s & (**e**) Ni 2p core level spectra of 3D flower-like β-$Ni(OH)_2$.

The thermal behavior of the as-prepared 3D flower-like β-$Ni(OH)_2$ was examined by TGA and DTA (Figure S5). The TGA curve of the 3D flower-like β-$Ni(OH)_2$ showed two weight-loss regions. The first weight-loss region was observed at ~240 to ~300 °C, which was attributed to the desorption of physisorbed water on the $Ni(OH)_2$ surface. The second weight-loss region was in the range, 300 to 480 °C. A large endothermic peak was observed at 300 °C for the sample in the DTA curves. The temperature range of the endothermic peak in the DTA curve fitted well with that of the weight loss in the TGA curve, corresponding to endothermic behavior during the decomposition of β-$Ni(OH)_2$ to NiO via the following reaction[33].

$$Ni(OH)_2 \rightarrow NiO + H_2O$$

The weight of the sample decreased continuously up to ~600 °C, after which no obvious weight loss was observed. The total weight loss below 500 °C was 20.6%, which is slightly higher than the theoretical value of 19.5% calculated from the decomposition reaction of $Ni(OH)_2$ to NiO, indicating that the complete decomposition of $Ni(OH)_2$ was achieved at 600 °C[21].

Electrochemical performance. The morphological effects of $Ni(OH)_2$-4, $Ni(OH)_2$-8, and 3D flower-like β-$Ni(OH)_2$ electrodes on the electrochemical capacitance were examined by CV and CD measurements, which is the most prominent tool for examining the capacitance property of the materials. CV is generally considered a suitable tool for determining the oxidation reduction behavior of the materials. Figure 5a presents the CV curves of the $Ni(OH)_2$-4, $Ni(OH)_2$-8, and 3D flower-like β-$Ni(OH)_2$ electrodes, at a 5 mVs^{-1} scan rate over the potential range, 0.0 to 0.5V. Figure 5b shows the CV curves of the 3D flower-like β-$Ni(OH)_2$ and Figure S6a,b shows the CV curve of the $Ni(OH)_2$-4 and $Ni(OH)_2$-8 at various scan rates ranging from 5–200 mV s^{-1}. All CV curves showed a pair of redox peaks, such as the anodic peak (positive current density) at approximately ~0.45 V, due to the oxidation of $Ni(OH)_2$ to NiOOH, whereas the cathodic peak (negative current density) at approximately ~0.19 V was assigned to the reverse reduction process, suggesting that the specific capacitance characteristic is governed mainly by the Faradic process[34–36]. Among these prepared electrodes, the 3D flower-like β-$Ni(OH)_2$ electrode possessed a significantly larger enclosed area than that of the β-$Ni(OH)_2$-4 and β-$Ni(OH)_2$-8 electrodes. This enhanced performance of the 3D flower-like β-$Ni(OH)_2$ electrode might have two explanations: (i) the three dimensional structure of the 3D flower-like β-$Ni(OH)_2$, which provides a larger surface area and better pore size than pure β-$Ni(OH)_2$-4 and β-$Ni(OH)_2$-8 (Figure S4), and can expose more active sites for the intercalation of ions; and (ii) the oriented crystallinity of 3D flower-like β-$Ni(OH)_2$ with a homogeneous elemental distribution may also enhance those electron intercalation/deintercalation processes (Figs 2 and S2).

The specific capacitance was examined further by CD to highlight the capacitance of the β-$Ni(OH)_2$-4, β-$Ni(OH)_2$-8, and 3D flower-like β-$Ni(OH)_2$ over the potential range, 0.0 to 0.4 V. Figure 5c presents the CD curve of β-$Ni(OH)_2$-4, β-$Ni(OH)_2$-8, and 3D flower-like β-$Ni(OH)_2$ at a fixed current density at 1 A g^{-1}. The 3D flower β-$Ni(OH)_2$ showed much higher capacitance performance ~1567 F g^{-1} at a current density of 1 A g^{-1} than the β-$Ni(OH)_2$-4, β-$Ni(OH)_2$-8, which is ~360 F g^{-1} and 1145 F g^{-1}, respectively, and might be due to its unique 3D flower-like structure. Furthermore, Fig. 5d shows the charge/discharge curves of the 3D flower-like β-$Ni(OH)_2$, whereas Figure S7a,b shows β-$Ni(OH)_2$-4 and β-$Ni(OH)_2$-8 at different current densities from 1 to

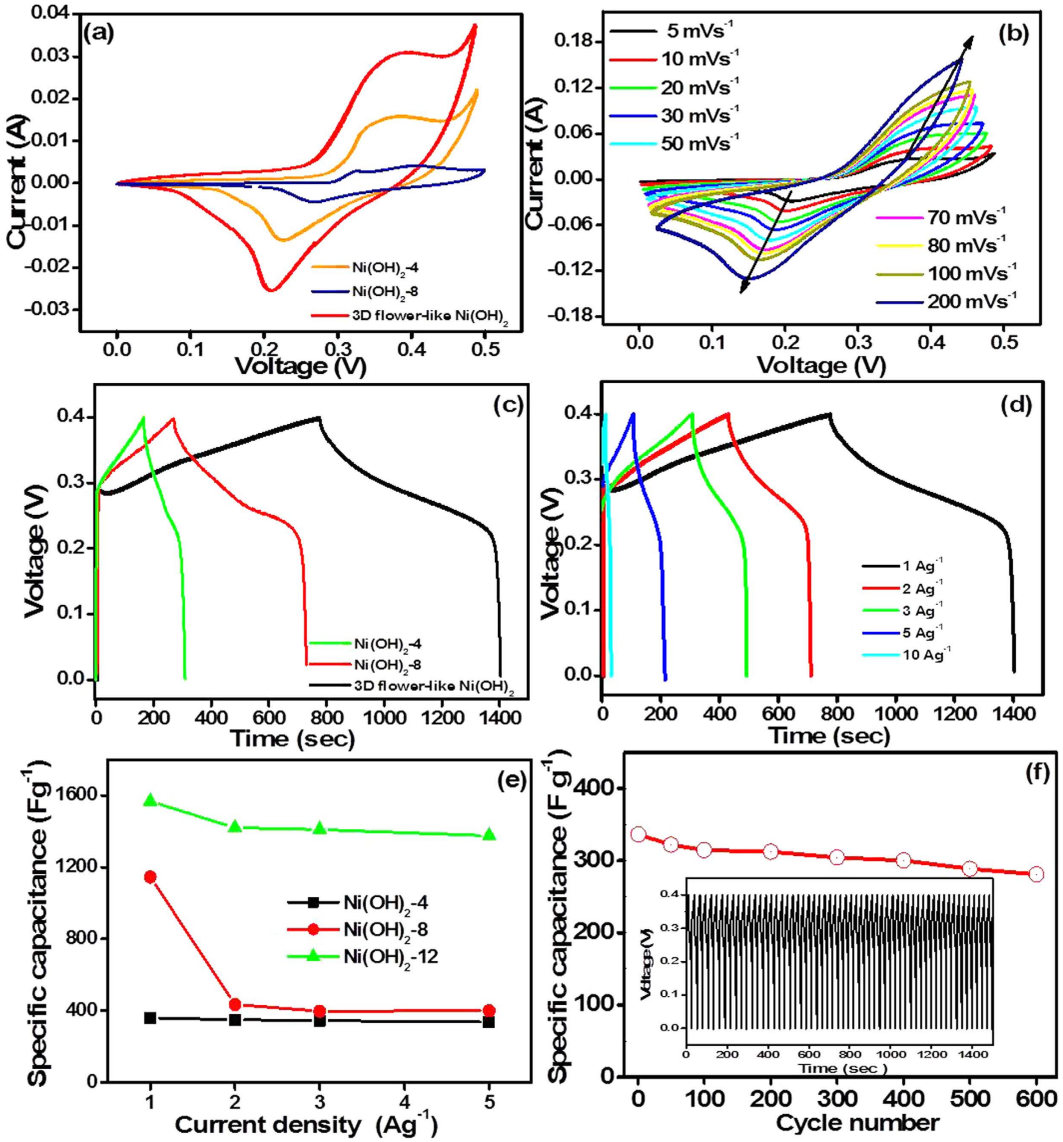

Figure 5. Electrochemical characterization of β-$Ni(OH)_2$: (**a**) Cyclic voltammograms of $Ni(OH)_2$-4, $Ni(OH)_2$-8 and 3D flower-like $Ni(OH)_2$ at a scan rate of 5 mV s^{-1} (**b**) 3D flower-like β-$Ni(OH)_2$ at a scan rate of 5–200 mV s^{-1}, (**c**) CD curves at a current density of 1 A g^{-1} (**d**) CD curves of 3D flower-like β-$Ni(OH)_2$ at different current densities, (**e**) specific capacitance of $Ni(OH)_2$-4, $Ni(OH)_2$-8 and 3D flower-like β-$Ni(OH)_2$, and (**f**) cyclic stability of 3D flower-like β-$Ni(OH)_2$.

10 A g^{-1}. The specific capacitance of β-$Ni(OH)_2$-4 at a current density of 1, 2, 3, 5, and 10A g^{-1} was found to be 360, 350, 345, 337, and 225 F g^{-1}, respectively, whereas for β-$Ni(OH)_2$-8, it was 1145, 435, 400, 397, and 275 F g^{-1}, respectively. Similarly, the specific capacitance of the 3D flower-like β-$Ni(OH)_2$ was ~1567, 1420, 1410, 1375, and 336 F g^{-1} at a current density of 1, 2, 3, 5, and 10 A g^{-1}. In particular, the 3D flower β-$Ni(OH)_2$ exhibited excellent capacitance performance because of its unique 3D structure, which provides a large surface area and better pore size that may offer more active sites for the intercalation of the electrolyte and can maximize its utilization as an electrode material. Furthermore, 3D flower-like β-$Ni(OH)_2$ retained ~25% capacitance, even at a high current rate of 10 A g^{-1}. Figure 5e presents the specific capacitance plotted as a function of the current density for β-$Ni(OH)_2$. The specific capacitance decreased with increasing current density owing to the decreased the penetration of the electrolyte into the pores of the electrode materials. For the 3D flower-like β-$Ni(OH)_2$, the apparent plateau region was observed at voltages greater than 0.4 V at a low current density of 1 A g^{-1} due to the oxidation of $Ni(OH)_2$ to NiOOH (Fig. S8), which is consistent with the CV results[11,37–42]. Table 1 lists the difference in capacitance between the 3D flower-like β-$Ni(OH)_2$ and other reported α-$Ni(OH)_2$ and β-$Ni(OH)_2$-based materials. Compared to previous reports, the 3D flower-like β-$Ni(OH)_2$ exhibited better performance than most of the capacitors reported previously.

Figure 5f represents the specific capacitances of 3D flower-like β-$Ni(OH)_2$ according to the cycling condition at a current density of 10 A g^{-1}. The specific capacitance of 3D flower-like β-$Ni(OH)_2$ (Fig. 5f) was as high as

S. no.	Structural morphology	Electrolyte	Specific Capacitance F g^{-1}	Current density A g^{-1}	Cyclic stability		Ref.
					Cycle Number	Retention %	
1	NiO	6M KOH	555	2	2000	–	11
2	$Ni(OH)_2$ nanospheres	1M KOH	694.5	1	1000	90	37
3	$Ni(OH)_2$ nanoplates	2M NaOH	793	1	–	–	38
4	$Ni(OH)_2$ nanoparticles	2M KOH	291	0.5 mA cm^{-2}	500	82	39
5	Hexagonal $Na(OH)_2$	3M KOH	578	2.5 mA	400	95	40
6	β-$Ni(OH)_2$ nanoparticles	1M KOH	715.3	0.5	–	–	41
7	$Ni(OH)_2$ nanowires	6M KOH	833	5 mA cm^{-2}	–	–	42
8	3D flower-like β-$Ni(OH)_2$	2M KOH	1567	1	600	90	Present work

Table 1. Comparative capacitance of 3D flower-like β-$Ni(OH)_2$ with other reported α and β-$Ni(OH)_2$ structures.

90% after 600 cycles. This suggests that the self-assembled building blocks of 3D flower-like β-$Ni(OH)_2$ may be more beneficial to enhancing the electrochemical performance than other morphologies, such as nanoparticles, nanoplates, nanospheres, etc. The excellent electrochemical performance of the as-prepared 3D flower-like β-$Ni(OH)_2$ is due to their unique structure. The 3D structure may contribute to the improved electrochemical performance. The open space between the adjacent sheets allows for the easy diffusion of the electrolyte, which ensures that every sheet can participate in the electrochemical reaction because every sheet is in contact with the electrolyte. The 3D structure composed of the centrifugally self-assembled nanosheets could effectively increase the electrode/electrolyte contact area and facilitate the rapid transport of ions and electrons. The high specific surface area and self-assembled sheets structures during the charge-discharge process are beneficial for the better electrical conductivity and high structural stability, leading to the high specific capacitance, and good cycling performance of the 3D flower-like β-$Ni(OH)_2$. The outstanding performance of the 3D flower-like β-$Ni(OH)_2$ can be attributed due to the unique self-assembled sheet-like structures shortening the diffusion length of the electrons and ions, and the large-area material-electrolyte contact. Their comparatively large surfaces can also benefit the charge-transfer rate. Therefore, in addition to the intrinsic nature of the materials, the superior electrochemical properties of the 3D flower-like β-$Ni(OH)_2$ originate from their large specific surface area and unique structure.

Conclusions

A one-pot oleylamine-assisted solvothermal approach was used to fabricate 3D flower-like β-$Ni(OH)_2$ assembled by a 2D sheet framework. The proposed methodology is a simple, single-step synthesis, and more importantly, oleylamine acts as both a reducing agent and surfactant in the synthesis process. The advantageous properties associated with the 3D flower-like structure are the larger surface area and better pore size, which can expose more active sites for the intercalation of ions, and the crystallinity of the 3D flower-like β-$Ni(OH)_2$ with a homogeneous distribution of elements also enhances the intercalation/deintercalation process leading to outstanding electrochemical properties, such as high specific capacitance, capability, and charge/discharge stability of the 3D flower-like β-$Ni(OH)_2$. The unique flower-like structures of β-$Ni(OH)_2$ can be extended further to a wide range of applications, such as sensors, electronic devices, hydrogen storage, catalysis, and lithium-ion batteries.

Experimental

Materials. Nickel nitrate ($Ni(NO_3)_2.6H_2O$), oleylamine ($C_{18}H_3NH_2$), and cyclohexane (C_6H_{12}) were acquired from Sigma Aldrich, South Korea. Methyl alcohol and ethyl alcohol were supplied by Duksan Pure Chemicals Co. Ltd., South Korea and used as received. The de-ionized water used in these experiments was obtained from a PURE ROUP 30 water purification system.

Methods. The changes in morphology from sheet to 3D flower-like β-$Ni(OH)_2$ were observed by scanning electron microscopy (SEM, HITACHI-S4800) and the internal structure of β-$Ni(OH)_2$ was examined by field emission transmission electron microscopy (FE-TEM, Tecnai G2 F20, FEI, USA). Phase analysis was performed by X-ray diffraction (XRD, PANalytical, X'Pert-PRO MPD, Netherland) using Cu Kα radiation ($\lambda = 0.15405$ nm). The functional groups and their interactions were examined by Fourier transform infrared (FTIR, Excalibur series FTS 3000 Bio-Rad spectrometer) spectroscopy. The textural properties were measured according to a N_2 adsorption-desorption method using a volumetric gas adsorption apparatus (ASAP 2020, Micromeritics Inc. USA). The chemical state and surface composition were analyzed by X-ray photoelectron spectroscopy (XPS, ESCALAB 250 XPS system, Thermo Fisher Scientific U.K.) using monochromatized Al l Kα ($h\nu = 1486.6$ eV). Thermogravimetric analysis (TGA, Perkin Elmer, Pyris Diamond) was performed by heating the samples from 20 °C to 800 °C at a rate of 10 °C/min with an air flow rate of 200 mL min^{-1}. The electrochemical properties were examined by cyclic voltammetry (CV) and charge/discharge (CD) using a potentiostat (Versa STAT 3, Princeton Research, USA).

Experimental details for the synthesis of β-$Ni(OH)_2$ nanostructures. The β-$Ni(OH)_2$ nanostructures were synthesized by adapting the oleylamine-assisted hydrolysis of aqueous nickel nitrate with the assistance of a solvothermal method based on "bottom up" approach chemistry. In a typical preparation of β-$Ni(OH)_2$, 1mM

$Ni(NO_3)_2.6H_2O$ and 20 ml ethanol were placed in a beaker with magnetic stirring for 10 min. Subsequently, 2 ml of oleylamine and 15 ml of ethanol were added to form the precursor solution of the nickel oleylamine complex. The homogeneous solution was then transferred to a 100 mL Teflon-lined autoclave. The autoclave was sealed and maintained at 180 °C for different times (4 to 12 h) and cooled to room temperature. The green samples were collected and washed rapidly with cyclohexane, distilled water and ethanol to remove the organics, ions, and possible impurities. The samples were then dried at 80 °C for 6 h. The samples prepared at different times, such as after 4h, 8h, and 12h, were labeled β-$Ni(OH)_2$-4, β-$Ni(OH)_2$-8, and 3D flower-like β-$Ni(OH)_2$, respectively

Electrode preparation and electrochemical measurements. All electrochemical measurements were taken on a potentiostat Versa STAT 3, Princeton Research, USA. The electrochemical tests were carried out in a three-electrode cell with an aqueous 2M KOH solution as the electrolyte and a Pt plate and a saturated AgCl/Ag (3M KCl) as the counter and reference electrodes, respectively. The active electrodes (β-$Ni(OH)_2$-4, β-$Ni(OH)_2$-8, and 3D flower-like β-$Ni(OH)_2$ were prepared by mixing the electroactive material (90 wt.%) and polytetrafluoroethene (10 wt.%) with isopropyl alcohol and pasted on nickel foam. Cyclic voltammetry (CV) was performed at scan rates of 5 mVs^{-1}-200 mVs^{-1} over the potential range, 0 to 0.5V. The galvanostatic charge-discharge (CD) measurements were carried out at current densities ranging from 1 A g^{-1} to 10 A g^{-1} and a potential window of 0 to 0.4 V. The integrated-average gravimetric capacitance of each electrode was calculated from the charge discharge equation[2].

References

1. Zhang, C., Lv, W., Tao, Y. & Yang, Q. H. Towards superior volumetric performance: design and preparation of novel carbon materials for energy storage. *Energy Environ. Sci.* **8,** 1390–1403 (2015).
2. Ansari, S. A., Parveen, N., Han, T. H., Ansari, M. O. & Cho, M. H. Fibrous polyaniline@manganese oxide nanocomposites as supercapacitor electrode materials and cathode catalysts for improved power production in microbial fuel cells. *Phys. Chem. Chem. Phys.* **18,** 9053–9060 (2016).
3. Simon, P. & Gogotsi, Y. Materials for electrochemical capacitors. *Nature Mater.* **7,** 845–854 (2008).
4. Parveen, N., Mahato, N., Ansari, M. O. & Cho, M. H. Enhanced electrochemical behavior and hydrophobicity of crystalline polyaniline@graphene nanocomposite synthesized at elevated temperature. *Composites Part B.* **87,** 281–290 (2016).
5. Mak, W. F. *et al.* High-energy density asymmetric supercapacitor based on electrospun vanadium pentoxide and polyaniline nanofibers in aqueous electrolyte. *J. Electrochem. Soc.* **159,** A1481–A1488 (2012).
6. Sugimoto, W., Iwata, H., Yasunaga, Y., Murakami, Y. & Takasu, Y. Preparation of ruthenic acid nanosheets and utilization of its interlayer surface for electrochemical energy storage. *Angew. Chem. Int. Ed.* **42,** 4092–4096 (2003).
7. Zhu, Y. *et al.* Ultrathin nickel hydroxide and oxide nanosheets: synthesis, characterizations and excellent supercapacitor performances. *Sci Rep.* **4,** 5787 (2014).
8. Li, W. *et al.* Facile synthesis of three-dimensional structured carbon fiber-$NiCo_2O_4$-$Ni(OH)_2$ high-performance electrode for pseudocapacitors. *Sci Rep.* **5,** 9277 (2015).
9. Cheng, Z. *et al.* High performance electrochemical capacitors based on MnO_2/activated-carbon-paper. *J. Mater. Chem. C.* **3,** 6166–6171 (2015).
10. Dubal, D. P., Fulari, V. J. & Lokhande, C. D. Effect of morphology on supercapacitive properties of chemically grown β-$Ni(OH)_2$ thin films. *Microporous Mesoporous Mater.* **151,** 511–516 (2012).
11. Li, X. *et al.* NiO ultrathin nanowire networks topotactically transformed from α-$Ni(OH)_2$ hierarchical microspheres and their superior electrochemical capacitance properties and excellent capability for water treatment. *J. Mater. Chem.* **22,** 14276–14283 (2012).
12. Wang, Q. H. *et al.* Facile synthesis and superior supercapacitor performances of three-dimensional cobalt sulfide hierarchitectures. *CrystEngComm.* **13,** 6960–6963 (2011).
13. Chang, J., Sun, J., Xu, C. H., Xu H. & Gao, L. Template-free approach to synthesize hierarchical porous nickel cobalt oxides for supercapacitors. *Nanoscale* **4,** 6786–6791 (2012).
14. Ci, S. *et al.* NiO-micro flower formed by nanowire-weaving nanosheets with interconnected Ni-network decoration as supercapacitor electrode. *Sci Rep.* **5,** 11919 (2015).
15. Ma, S. B. *et al.* A novel concept of hybrid capacitor based on manganese oxide materials. *Electro. chem. Commun.* **9,** 2807–2811 (2007).
16. Lee, J. W., Ko, J. M. & Kim, J. D. Hierarchical microspheres based on α-$Ni(OH)_2$ nanosheets intercalated with different anions: synthesis, anion exchange, and effect of intercalated anions on electrochemical capacitance. *J. Phys. Chem. C.* **115,** 19445–19454 (2011).
17. Li, L. *et al.* The facile synthesis of hierarchical porous flower-like $NiCo_2O_4$ with superior lithium storage properties. *J. Mater. Chem. A.* **1,** 10935–10941 (2013).
18. Zhong, L. S. *et al.* Self-assembled 3D flowerlike iron oxide nanostructures and their application in water treatment. *Adv. Mater.* **18,** 2426–2431 (2006).
19. Xia, Y. A., Xiong, Y. J., Lim, B. K. & Skrabalak, S. E. Shape-controlled synthesis of metal nanocrystals: simple chemistry meets complex physics. *Angew. Chem. Int. Ed.* **48,** 60–103 (2009).
20. Chen, H., Hu, L. F., Chen, M., Yan, Y. & Wu, L. M. Nickel cobalt layered double hydroxide nanosheets for high-performance supercapacitor electrode materials. *Adv. Funct. Mater.* **24,** 934–942 (2014).
21. Ping, L. *et al.* Self-assembled 3D flower-Like hierarchical β-$Ni(OH)_2$ hollow architectures and their *in situ* thermal conversion to NiO. *Nanoscale Res. Lett.* **4,** 550–557 (2009).
22. Hajrya, A. A. *et al.* Low-temperature growth and properties of flower-shaped β-$Ni(OH)_2$ and NiO structures composed of thin nanosheets networks. *Superlattices Microstruct.* **44,** 216–222 (2008).
23. Tong, G. X. *et al.* Polymorphous α- and β-$Ni(OH)_2$ complex architectures: morphological and phasal evolution mechanisms and enhanced catalytic activity as non-enzymatic glucose sensors. *CrystEngComm.* **14,** 5963–5973 (2012)
24. Liu, J. *et al.* A non-sulfided flower-like NiPTA catalyst that enhances the hydro treatment efficiency of plant oil to produce green diesel. *Sci Rep.* **5,** 15576 (2015).
25. Jeevanandam, P., Koltypin, Yu. & Gedanken, A. synthesis of nanosized α-nickel hydroxide by a sonochemical method. *Nano Lett.* **1,** 263–266 (2001).
26. Cai, S. F. *et al.* $Ni(OH)_2$ Tubes with mesoscale dimensions as positive-electrode materials of alkaline rechargeable batteries. *Angew. Chem. Int. Ed.* **43,** 4212–4216 (2004).
27. Sarkar, S. *et al.* An aminolytic approach toward hierarchical β-$Ni(OH)_2$ nanoporous architectures: A bimodal forum for photocatalytic and surface-enhanced raman scattering activity. *Inorg. Chem.* **49,** 8813–8827 (2010).

28. Zhu, G. *et al.* Polymer guided synthesis of $Ni(OH)_2$ with hierarchical structure and their application as the precursor for sensing materials. *CrystEngComm*. **15,** 9189–9195 (2013).
29. Liu, Y. *et al.* Hierarchical $CoNiO_2$ structures assembled from mesoporous nanosheets with tunable porosity and their application as lithium-ion battery electrodes. *New J. Chem*. **38,** 3084–3091 (2014).
30. Liu, Z. Q. *et al.* Facile hydrothermal synthesis of urchin-like $NiCo_2O_4$ spheres as efficient electro catalysts for oxygen reduction reaction. *In. J. of hydrogen energy* **38,** 6657–6662 (2013).
31. Payne, B. P., Biesinger, M. C. & McIntyre, N. S. Use of oxygen/nickel ratios in the XPS characterization of oxide phases on nickel metal and nickel alloy surfaces. *J. of Electron Spectroscopy and Related Phenomena* **185,** 159–166 (2012).
32. Marco, J. F., Gancedo, J. R. & Gracia, M. Characterization of the nickel cobaltite, $NiCo_2O_4$, prepared by several methods: An xrd, xanes, exafs, and xps Study. *J. of Solid State Chem*. **153,** 74–81 (2000).
33. Cheng, B., Le, Y., Cai, W. & Yu, J. Synthesis of hierarchical $Ni(OH)_2$ and NiO nanosheets and their adsorption kinetics and isotherms to congo red in water. *J. Hazard. Mater.* **185,** 889–897 (2011).
34. Lu, Z., Chang, Z., Zhu, W. & Sun, X. β phase $Ni(OH)_2$ nanowall film with reversible capacitance higher than theoretical faradic capacitance. *Chem. Comm*. **47,** 9651–9653 (2011).
35. Zhu, Y. *et al.* Ultrathin nickel hydroxide and oxide nanosheets: synthesis, characterizations and excellent supercapacitor performances. *Sci. rep.* **4,** 5787 (2014).
36. Zhang, L. *et al.* Flexible hybrid membranes with $Ni(OH)_2$ nanoplatelets vertically grown on electro spun carbon nanofibers for high-performance supercapacitors. *ACS Appl. Mater. Interfaces* **7,** 22669–22677 (2015).
37. Tizfahma, J. *et al.* Supercapacitive behavior of β-$Ni(OH)_2$ nanospheres prepared by a facile electrochemical method. *Colloids and Surfaces A: Physicochem. Eng. Aspects* **443,** 544–551 (2014).
38. Ren, Y. *et al.* Hydrothermal synthesis of β-$Ni(OH)_2$ nanoplates as electrochemical pseudocapacitor materials. *Int. J. Electro chem. Sci.* **7,** 12236–12243 (2012).
39. Vijayakumar, S. & Muralidharan, G. Electrochemical supercapacitor behavior of α-$Ni(OH)_2$ nanoparticles synthesized via green chemistry route. *J. of Electro analytical Chem*. **727,** 53–58 (2014).
40. Zhao, D. D., Bao, S. J., Zhou, W. J. & Li, H. L. Preparation of hexagonal nanoporous nickel hydroxide film and its application for electrochemical capacitor. *Electro chem. Comm*. **9,** 869–874 (2007).
41. Aghazadeh, M., Golikand, A. N. & Ghaemi, M. Synthesis, characterization, and electrochemical properties of ultrafine β-$Ni(OH)_2$ nanoparticles. *Inter. J. hydrogen energy* **36,** 8674–8679 (2011).
42. Wang, Y. X., Hub, Z. & Wu, H. Y. Preparation and electrochemical performance of α-nickel hydroxide nanowire. *Material Chem. and Phy*. **126,** 580–583 (2011).

Acknowledgements

This study was supported by the Priority Research Centers Program (NRF Grant No: 2014R1A6A1031189), and by Basic Science Research Program (NRF Grant No: 2015R1D1A3A03018029) through the National Research Foundation of Korea (NRF) funded by the Ministry of Education.

Author Contributions

N.P. and M.H.C. conceived, designed, performed the experiments, wrote the manuscript and checked the English grammars in manuscript.

Additional Information

Supplementary information accompanies this paper at http://www.nature.com/srep

Competing financial interests: The authors declare no competing financial interests.

How to cite this article: Parveen, N. and Cho, M. H. Self-Assembled 3D Flower-Like Nickel Hydroxide Nanostructures and Their Supercapacitor Applications. *Sci. Rep.* **6**, 27318; doi: 10.1038/srep27318 (2016).